Size Effects on the Bending Behaviour of Reinforced Concrete Beams

Brincker, Rune; Henriksen, M. S.; Christensen, F. A.; Heshe, Gert

Published in:
Minimum Reinforcement in Concrete Members

Publication date:
1999

Document Version
Publisher's PDF, also known as Version of record

after the concrete tension failure peak seems to be well estimated by the model, indicating that it seems reasonable to assume a constant frictional shear stress in the debonded zones at each side of the crack.

References

1. Hillerborg A., M. Modeer and P.E. Peterson (1976): Analysis of Crack Formation and Crack Growth in Concrete by means of Fracture Mechanics and Finite Elements. *Cement and Concrete Research* **6**, pp. 773-782.
2. Bosco C. and A. Carpinteri (1992): Fracture Mechanics Evaluation of Minimum Reinforcement in Concrete Structures. In: *Applications of fracture Mechanics to Reinforced Concrete*, ed. A. Carpinteri, Elsevier, London, pp. 347-377.
3. Baluch M.H., A.K. Azad and W. Ashmawi (1992): Fracture Mechanics Application to Reinforced Concrete Members in Flexure. In: *Applications of Fracture Mechanics to Reinforced Concrete*, ed. A. Carpinteri, Elsevier, London, pp. 413-436.
4. Hawkins N.M. K. and Hjorteset (1992): Minimum Reinforcement Requirements for Concrete Flexural members. In: *Applications of Fracture Mechanics to Reinforced Concrete*, ed. A. Carpinteri Elsevier London, pp. 379-412.
5. Hededal O. and I. Kroon (1991): Lightly Reinforced High-Strength Concrete. M.Sc. Thesis in Civil Engineering, Department of Building Technology and Structural Engineering, Aalborg University, Denmark.
6. Planas J., G. Ruiz and M. Elices (1995): Fracture of Lightly Reinforced Concrete Beams. In: *Theory and Experiments In Fracture Mechanics of Concrete Structures*, ed. F.H. Wittmann, Proc. of FRAMCOS-2 Conference, pp. 1179-1188.
7. Petersson P.E. (1981): Crack Growth and Development of Fracture Zones in Concrete and Similar Materials. Ph.D. thesis, Lund Institute of Technology, Sweden.
8. Brincker R. and H. Dahl (1989): Fictitious Crack Model of Concrete Fracture. *Magazine of Concrete Research* **41** ,No. 147, pp. 79-86.

APPENDIX C:

MULTIPLE CRACKING AND ROTATIONAL CAPACITY OF LIGHTLY REINFORCED BEAMS

Prepared by F.A. Christensen, M.S. Henriksen and R. Brincker

Abstract

In this appendix a model is formulated for the rotational capacity of reinforced concrete beams assuming rebar tension failure. The model is based on a classical approach and establishes the load-deflection curve of a reinforced concrete beam. The rotational capacity is then obtained as the area under the load-deflection curve divided by the yield moment of the beam. In calculating the load deflection curve, the cracking process of the concrete is ignored. By assuming that all cracks are fully opened, the energy dissipated during cracking of the concrete is taken into account by simply adding the total tensile fracture energy to the total plastic work obtained by the classical analysis.

Model Formulation

Before cracking of the concrete both the concrete and the reinforcement are assumed to behave elastically, and no slip is assumed between concrete and reinforcement. Assuming a linear variation of the normal beam strain over the cross-section, the stress distribution is obtained by classical beam theory.

When the tensile strength is reached at the tensile side of the beam, the concrete is assumed to crack. Further, cracks are assumed to be formed during constant bending moment (no decrease of the bending moment) and are allowed to extend until the level of the neutral axis. The tension force from the reinforcement is balanced by compression stresses in the concrete. The size of the compression zone is obtained by assuming a uniform distribution of the compression stresses and using an equilibrium equation. At the cracked section the tensile force in the reinforcement is transferred to the surrounding concrete by assuming a formation of two debonded zones around the crack with constant shear friction τ_f. In Figure C1 the stress distribution at a cracked section of the beam is shown immediately before and after formation of a crack.

Calculation Procedure

The crack development is initiated when the tensile strength is reached at the tensile side of the beam in the cross section with maximum bending moment. This corresponds to the situation shown in Figure C1. As the load increases, cracks might form in neighbour sections. If the bending moment is equal to the cracking moment at section II a new crack will be formed at section II. If the bending moment is less than the cracking moment, the load is increased causing the debonded zones to extend. By repeating this procedure cracks are formed one by one until tensile

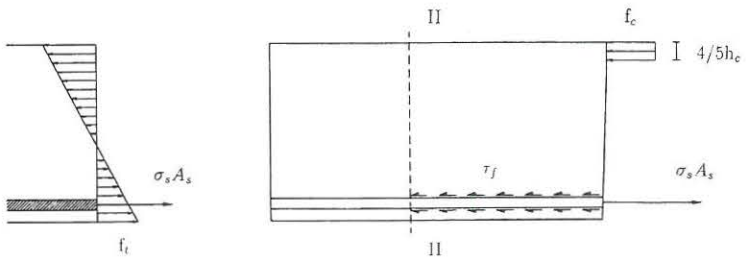

Figure C1. Stress distribution in cracked and uncracked cross-section. The debonded zone with constant shear friction stress ends at section II.

failure of the reinforcement bar. At the time a new crack is formed it is assumed that the strain at section II in Figure C1 is the same in the concrete and in the reinforcement and that the strain is equal to the tensile fracture strain of the concrete ($\epsilon = f_t/E_c$).

The load-deflection curve is found by integrating the curvature over the length of the beam. A typical load-deflection curve is shown in Figure C2. The curvature is determined as the ratio between the reinforcement strain and the distance from the reinforcement to the neutral axis at the cracked sections.

The rotational capacity is calculated by integrating the load deflection curve and adding the energy dissipated in the crack formation process estimated as nA_cG_F where n is the number of cracks, A_c is the cross sectional area of the beam and G_F is the fracture energy of the concrete.

Model Properties

Investigating the model properties, results have been derived using the following values for the material parameters:

$$
\begin{aligned}
f_y &: 500\ MPa \\
f_u &: 575\ MPa \\
\tau_f &: 5.0\ MPa \\
f_t\ (NSC) &: 3.0\ MPa \\
f_t\ (HSC) &: 5.0\ MPa \\
f_c\ (NSC) &: 60.0\ MPa \\
f_c\ (HSC) &: 90.0\ MPa \\
G_F &: 0.120\ N/mm \\
\epsilon_y &: 2.0\ \% \\
\epsilon_u &: 15.0\ \% \\
E_s &: 210{,}000\ MPa
\end{aligned}
$$

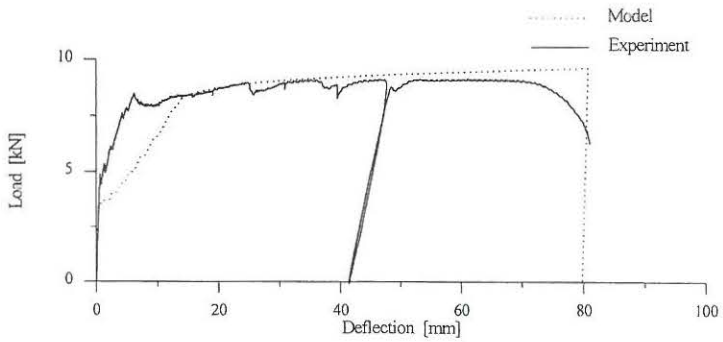

Figure C2. Failure response curve for 100 × 200 × 2400 mm beam with 0.14 % reinforcement compared with typical experimental result.

representative for the two types of concrete used in the experimental investigation, see Appendix A.

For this kind of model, one of the most important parameters is the amount of reinforcement strain hardening described by the ratio f_u/f_y. If no strain hardening is present, i.e. if the ratio $f_u/f_y = 1$, at each crack, only one point (the point situated just between the concrete tensile failure crack faces) can be in the state of yielding. Thus, since the length of the zone over which yielding takes place tends to zero when the ratio tends to 1, the rotational capacity tends to zero. Furthermore, in this case only one crack will be formed reducing the possibilities of energy dissipation even further. The results clearly support these considerations. Figure C3 shows that the rotational capacity is highly dependent upon the ratio f_u/f_y.

One would expect the results of the model to be rather sensitive to the value of the shear friction stress τ_f. However, this is not the case, Figure C4. Generally it can be stated that the rotational capacity decreases with increasing friction stress, although the influence is small. The energy dissipation due to yielding and debonding decreases with increasing values of the shear friction stress, but at the same time the number of cracks increases, and thus, the contribution from dissipation of energy in the concrete tensile cracks increases.

Figure C5 shows the results for a normal strength concrete and a high strength concrete. As it appears from the figure, increasing the concrete strength decreases the rotational capacity for all values of the reinforcement ratio.

For the value of shear friction stress used here, $\tau_f = 5MPa$, the model only shows a small size effect. For larger values of τ_f, introducing a relatively larger contribution from concrete tensile

fracture energy dissipation, somewhat larger size effects are observed, see the results in the main part of the chapter. However, the results in Figure C6 clearly show that the rotational capacity is non-sensitive to the size, but highly sensitive to the deformation capacity of the steel. For the low deformation capacity steel the value of the ultimate strain was reduced to $\epsilon_u = 2.0\%$, approximately equal to the failure strain of the cold deformed bars used in the experimental investigation, see Appendix A.

All Figures C3-C6 show how the rotational capacity is influenced by the reinforcement ratio. When reinforcement tensile failure controls the failure of the beam the rotational capacity is increasing with increasing reinforcement ratio.

Comparing with Experimental Results

Figure C7 and C8 show how the model compares with experimental results for the rotational capacity. In Figure C7 the case of normal strength concrete is shown.

In case of reinforcement ratios of 0.14% and 0.25% the model results fit the experiments well, whereas in some cases of 0.39% reinforcement ratio the experiments show that reinforcement tensile failure is no longer the dominating failure mode and therefore the model over-estimates the rotational capacity. The experimental results show, as the model, that the rotational capacity is higher in the case of normal strength concrete.

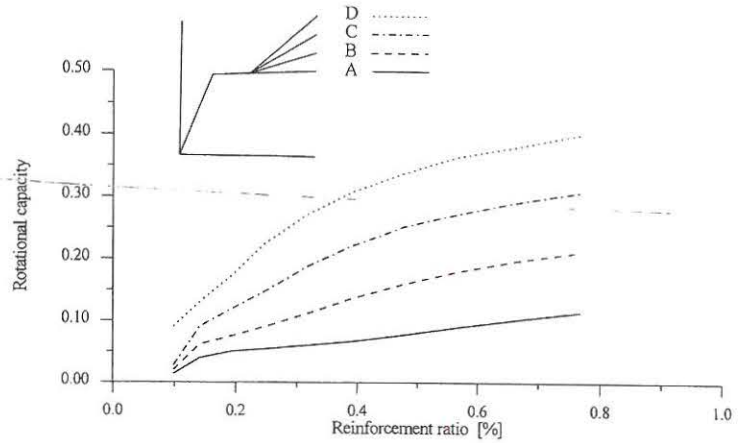

Figure C3. Rotational capacity as a function of the reinforcement ratio for different strain hardening properties A), B), C) and D) of the reinforcement.

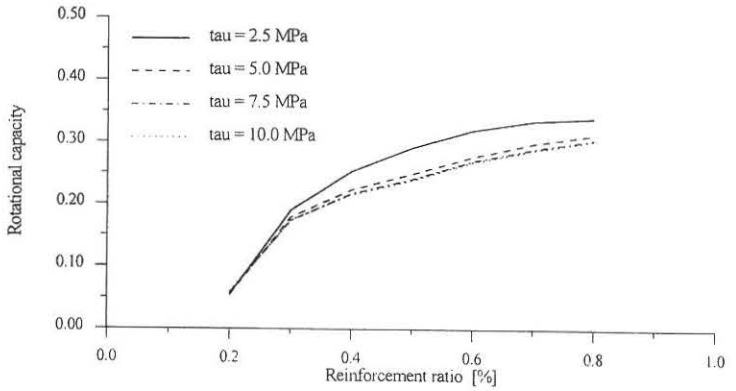

Figure C4. Rotational capacity as a function of the reinforcement ratio for different values of the debonding shear friction stress τ_f.

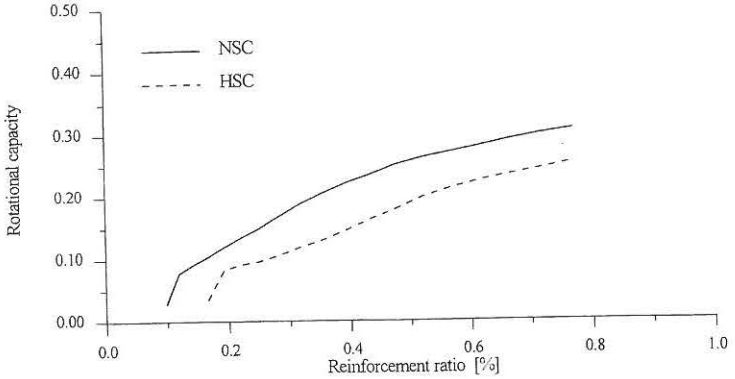

Figure C5. Rotational capacity as a function of the reinforcement ratio for normal strength concrete and high strength concrete.

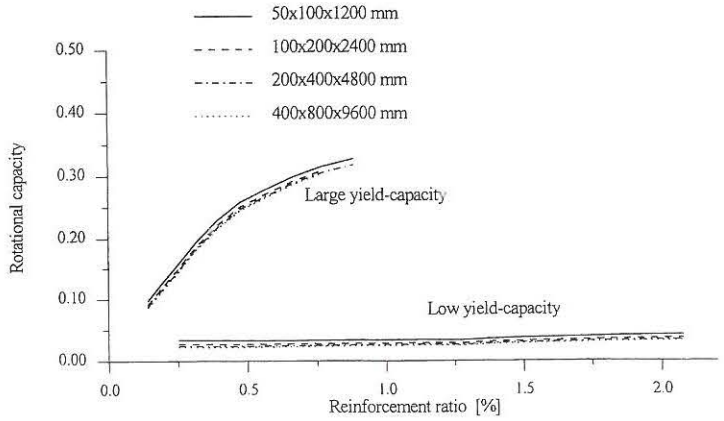

Figure C6. Size effect on the rotational capacity as a function of the reinforcement ratio for different reinforcement types: a low deformation capacity type, and a high deformation capacity type.

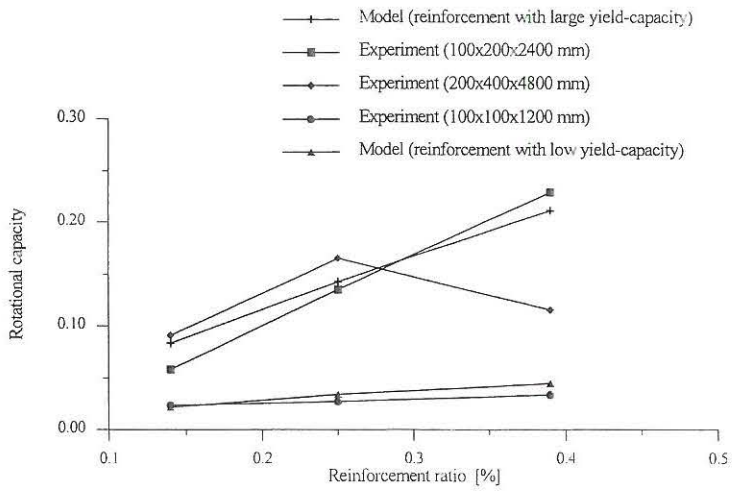

Figure C7. Comparison between rotational capacities obtained from model and from experiments (normal strength concrete).

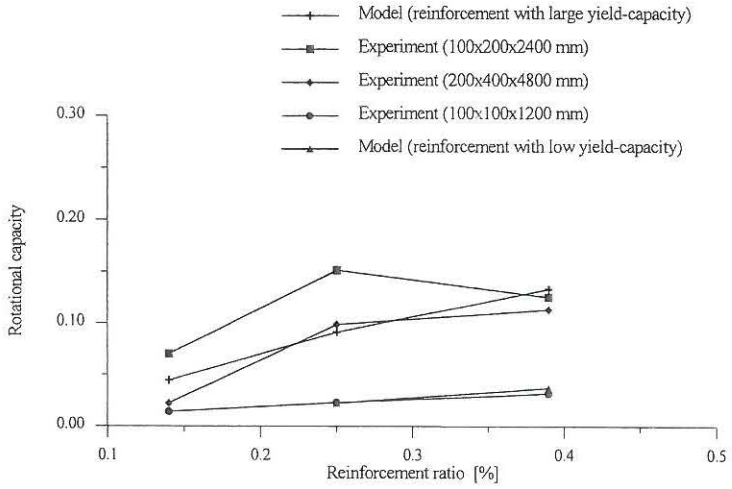

Figure C8. Comparison between rotational capacities obtained from model and from experiments (high strength concrete).

APPENDIX D:

FRACTURE MECHANICAL MODEL FOR ROTATIONAL CAPACITY OF HEAVILY REINFORCED CONCRETE BEAMS

Prepared by M.S. Henriksen, R. Brincker and G. Heshe

Abstract

In this appendix the flexural behaviour of reinforced concrete beams is investigated by analytical methods originally introduced by A. Hillerborg. A simple analytical model is presented which describes the bending moment-curvature relation for normal and over-reinforced beams taking into account the strain localization within the compression zone of the concrete. The strain softening part of the stress-strain curve for the concrete is described as a stress-deformation relation which is dependent on the length over which the compression failure extends along the beam axis. On the basis of the moment-curvature relation estimated by the model, the load-deflection curve is calculated, and the rotational capacity is obtained as the total plastic work divided by the yield moment of the beam. The results of the model are obtained assuming a linear compression softening curve with different values of the critical compression deformation and the fracture zone length. The results are compared with experiments.

Introduction

In the past ten years a lot of research has been carried out in the field of compression failure of reinforced concrete structures. After development of different crack models for the fracture in tension like the Fictitious Crack Model, Hillerborg was one of the researchers that began to investigate the softening behaviour of the fracture in compression [1],[2] and [3].

Hillerborg had already shown that the softening behaviour in tension was size-dependent, and inspired by the work of van Mier [4], Hillerborg got the idea of using the model for tension softening on compression failure. This led to a simple model describing the uniaxial stress-strain relation for concrete based on fracture mechanical concepts, Figure D1. The strain localization within the compression zone was taken into account by defining a characteristic length dependent on the depth of the compression zone.

Van Mier and Vonk at the Stevin Laboratory carried out different experimental studies on the full range behaviour in compressive loading of different concrete cubes as well as performed micro-mechanical modelling of the compression softening [4],[5]. Recent studies of the behaviour in compression of both normal strength concrete (45 MPa) and high strength concrete (90 MPa) have been presented by Jansen and Shah [6], who performed experimental investigations on cylinders with constant diameter and different depths to examine the effect of specimen depth on compressive strain softening of concrete, see Figure D2. Their results show that the post-peak

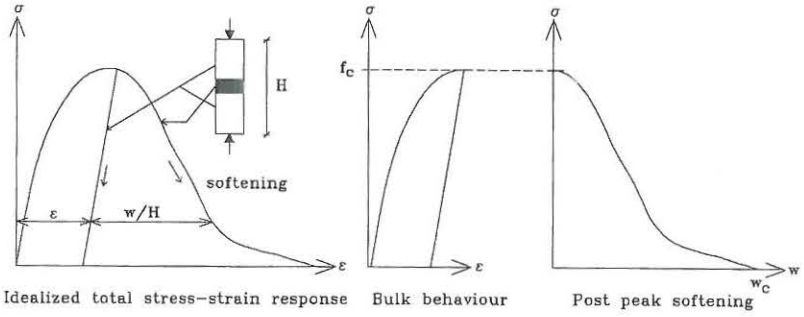

Figure D1. Basic idea of stress-strain relation in compression by Hillerborg [1].

behaviour including the post peak energy dissipation is relatively insensitive to the depth of the cylinder specimen.

Several researchers have examined the influence on compression softening behaviour when changing the depth of test cylinders and when using intermediate layers between the loading plate and the cylinder, but it seems to be a lack of investigations on the influence of changing the diameter. A so-called Compressive Damage Zone model has also been established by Markeset taking into account also localized shear deformation and deformation due to splitting cracks [7].

In this investigation, the length, over which the compression failure extends along the beam axis, is introduced as a characteristic length proportional to the depth of the compression zone $l_{ch} = \beta h_c$ and the softening is assumed to be linear. Thus, the model contains two parameters describing the basic fracture mechanical properties of the model: the characteristic length parameter β and a critical softening deformation w_c. In the following the influence of the parameters w_c and β on the full range behaviour of different model beams is analysed, and, based on the load-deflection curves, the rotational capacity is estimated as the total plastic work divided by the yield moment of the beam.

Basic Assumptions of the State of Compression Failure

When a reinforced concrete beam is loaded to ultimate compression failure and an unloading starts taking place, the critical cross-section is assumed to pass through three different states of failure, see Figure D3.

The continuum state for the critical cross-section describes an elastic state for the concrete where the concrete stresses $\sigma_c < f_c$ for all points in the cross-section. Varying the concrete strain ε_c from zero to the peak strain ε_0, the depth of the compression zone h_c will be constant. In this phase the reinforcement is assumed to be in an elastic state corresponding to $\sigma_s < f_y$.

The condition of fracture zone growth is satisfied when the concrete stress in the compressed edge

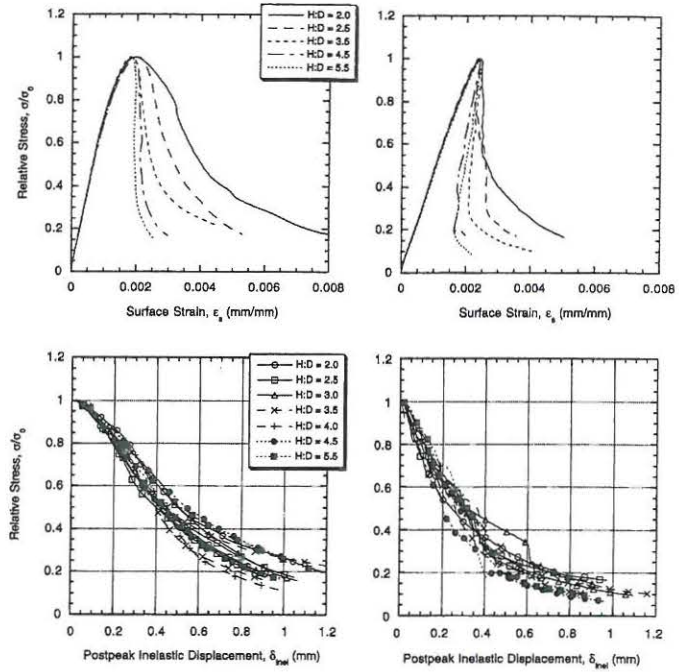

Figure D2. Influence of specimen length on concrete cylinder uniaxial compressive stress-strain curve, (diameter 100 mm). Left: Normal strength concrete (45 MPa). Right: High strength concrete (90 MPa). According to Jansen and Shah [6].

of the cross-section reaches the concrete compression strength. At this condition a fracture zone will start developing. When the fracture zone is fully developed, i.e. when the compression stress at the top of the beam has dropped to zero, the length of the fracture zone along the beam axis is assumed to be l_{ch}, where l_{ch} is defined as a characteristic length. The material within the fracture zone follows a softening branch and outside this zone an unloading takes place. The characteristic length could be assumed to be dependent on either the depth of the compression zone or on the width of the cross-section.

It is well known that the final compression failure of cylinders is often a so-called "cone-failure" where the concrete fails in a compression-shear mode with the development of slip-planes at an angle γ typically around $\gamma \cong 30°$. Thus, for a cylinder with radius r, the characteristic length might be defined as $l_{ch} \tan(\gamma) = 2r$, and then taking the approximation $\tan(\gamma) \cong 0.5$ we get $l_{ch} \cong 4r$, see Figure D4.

Following this idea, the failure mode of the compression zone of a beam is assumed to be a similar compression-shear mode with the development of slip-planes at a certain angle to horizontal. Now, assuming that the slip-planes will start at the point where the strain is zero, the characteristic length becomes proportional to the depth h_c of the compression zone, thus $l_{ch} = \beta h_c$. Assuming

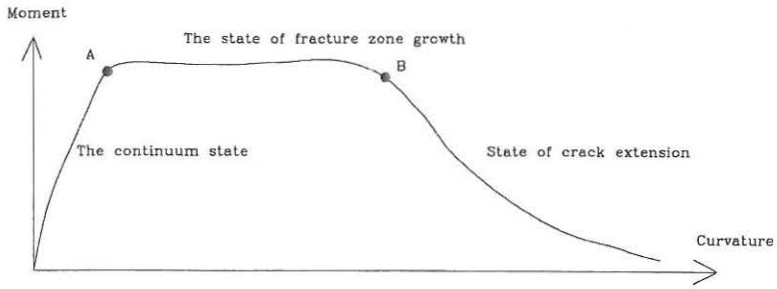

Figure D3. Full range behaviour for a reinforced concrete beam.

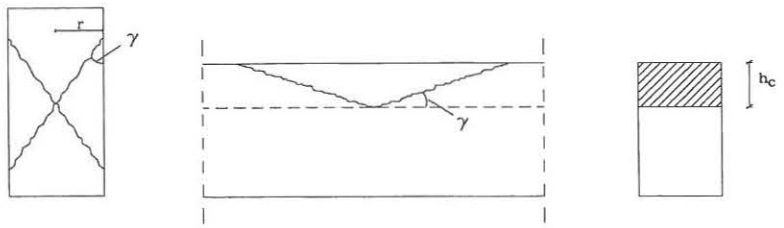

Figure D4. Definition of the parameter β describing the length of the failure zone. Left: Cone failure of a cylinder in compression. Right: Assumed failure mode in the compression zone of a beam in bending.

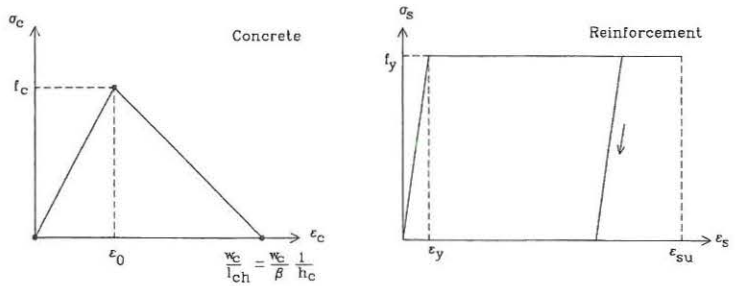

Figure D5. Simplified analytical stress-strain curves for the reinforcement and the concrete.

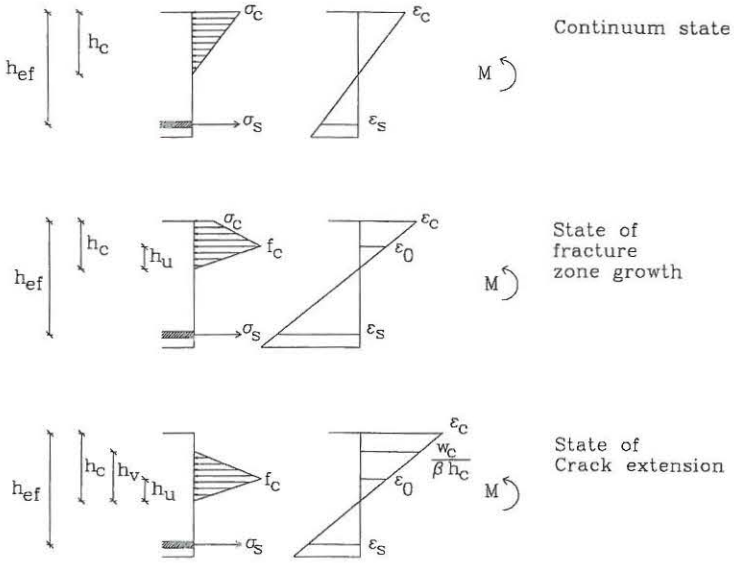

Figure D6. The stress and strain distribution for the critical cross-section.

that the slip-planes develop at an angle similar to the cylinder failure gives the estimate $\beta \cong 4$, Figure D4.

However, the relation $l_{ch} = \beta h_c$ is only expected to be valid on the assumption that the depth of the compression zone is small compared to the width b of the beam. If the beam width becomes substantially smaller than the depth of the compression zone, it is more reasonable to assume a failure mode where vertical slip-planes develop, and thus, for this case it should be assumed that the characteristic length is proportional to the width b of the beam. In the following however, the relation $l_{ch} = \beta h_c$ will be used.

Using the approach of a characteristic length l_{ch}, the softening deformation can be represented as a strain, and thus, the full range behaviour of both concrete and reinforcement can be represented by a stress-strain relation, Figure D5.

In the state of crack extension a part of the material in the compression zone has totally failed and a "real crack" is formed. The final failure develops as the crack extends downwards through the beam.

Modeling Flexural Behaviour

In the modeling it is assumed that the considered beams are subjected to three-point bending, and the critical cross-section is assumed to be reinforced only by main reinforcement. Thus, the

influence of compressive reinforcement and stirrups is not taken into account. The bending tensile strength of the concrete is set equal to zero which means that the cross-section is assumed to be cracked from the start. Effects from other cracks along the beam axis as well as bond-slip effects between the concrete and the reinforcement are not considered. For calculation of the full range behaviour Bernuoilli's assumption (plane cross-sections remain plane) is applied.

The model describing the full range behaviour is based on simplified linear stress-strain curves for the reinforcement and the concrete, see Figure D5. Typical stress and strain distributions for the critical cross-section and each of the fracture states are shown in Figure D6.

The flexural behaviour is described for the three states as non-dimensional moment-curvature relations as follows:

The continuum state, $\epsilon_c \leq \epsilon_0$

$$\frac{6M}{bh_{ef}^2 f_c}(\xi, \epsilon_c) = \left(3\xi - \xi^2\right)\frac{\sigma_c}{f_c} \tag{1}$$

the state of fracture zone growth, $\epsilon_0 < \epsilon_c \leq w_c/\beta h_c$

$$\frac{6M}{bh_{ef}^2 f_c}(\xi, \epsilon_c) = 3\xi + \left(\frac{\varepsilon_0}{\varepsilon_c} - 2\right)\xi^2 + \left(\left(3 - 3\frac{\varepsilon_0}{\varepsilon_c}\right)\xi - \left(1 + \frac{\varepsilon_0}{\varepsilon_c}\left(\frac{\varepsilon_0}{\varepsilon_c} - 2\right)\right)\xi^2\right)\frac{\sigma_c}{f_c} \tag{2}$$

and the state of crack extension, $\epsilon_c > w_c/\beta h_c$

$$\frac{6M}{bh_{ef}^2 f_c}(\xi, \epsilon_c) = \left(3\frac{w_c}{\beta h_c \varepsilon_c} + \frac{w_c^2}{(\beta h_c)^2 \varepsilon_c^2}\right)\xi + \left(2\frac{w_c \varepsilon_0}{\beta h_c \varepsilon_c^2} - 3\frac{w_c}{\beta h_c \varepsilon_c}\right)\xi^2 \tag{3}$$

where $\xi = h_c/h_{ef}$.

Bending moment-curvature curves and load-deflection curves are shown for different values of w_c and β in Figure D7. Here the curvature is calculated as the angle in the strain distribution ϵ_c/h_c. The results are shown for a reinforced normal strength concrete beam with reinforcement ratios (A_s/bh) 0.78 %, 1.57 %, 2.45 % and 4.02 %. Values for the beam dimensions are $b = 200\ mm$, $h = 400\ mm$, $l = 4800\ mm$. The concrete parameters are $f_c = 60\ MPa$, $\varepsilon_0 = 0.2$ % and the reinforcement parameters are $f_y = 600\ MPa$, $E_s = 2.0 \times 10^5\ MPa$, $\varepsilon_{su} = 10$ %. Note the large sensitivity of the modelled behaviour on the values of the two key parameters w_c and β.

Load-deflection curves are obtained by integrating the curvature distribution according to the principle of virtual work. When the curvature is integrated, it is kept constant over the characteristic length, see Figure D8 where the distribution of curvature along the beam axis is shown in the state of ultimate failure, here defined as the transition between the state of fracture zone growth and the state of crack extension.

The rotational capacity is estimated by integrating the load-deflection curves to obtain the total plastic work, and then dividing by the yield moment to obtain a non-dimensional parameter θ.

The parameter θ is a direct measure of the rotational capacity of the beam.

Results for the rotational capacity are shown in Figures D9-D12 for different values of w_c and β. As expected, the rotational capacity is strongly sensitive to both parameters. Note that since the ultimate strain of the reinforcement is incorporated in the analysis, some of the test results correspond to reinforcement tensile failure. The reason for incorporating this rather simple tension failure in this model (no bond-slip is modeled) is to have a rough check on the capability of the model to show a reasonable switch between the two modes of failure. The part of the rotational capacity curves in Figures D9-D12, where the rotational capacity is increasing with the reinforcement ratio, corresponds to reinforcement tension failure. This part of the results should be acknowledged as less interesting (modelling for this part is given in Appendix C) than the rest of the curve corresponding to concrete compression failure.

More details of the modelling are given in Henriksen and Brincker [8].

Comparison with Experimental Results

The values of the rotational capacity estimated by the model are shown in Figures D13-D16 as a function of the reinforcement ratio and compared with experimental results from Appendix A for normal strength concrete beams with a cross-section of 100 × 100 mm, 100 × 200 mm and 200 × 400 mm and slenderness number 12. As it appears, the best agreement is obtained for the values $w_c = 4$ mm and $\beta = 8$.

Figure D16 shows that using the values $w_c = 4$ mm and $\beta = 8$, the rotational capacity estimated by the model compares reasonably well with experimental results for all the three beam sizes.

References

1. Hillerborg, A. (1990): Fracture Mechanics Concepts Applied to Moment Capacity and Rotational Capacity of Reinforced Concrete Beams. *Engineering Fracture Mechanics* **35**, No. 1/2/3, pp. 233-240.
2. Hillerborg, A. (1988): Rotational Capacity of Reinforced Concrete Beams. *Nordic Concrete Research* **7**, pp. 121-134.
3. Hillerborg, A. (1991): Size Dependency of the Stress-Strain Curve in Compression. In: *Analysis of Concrete Structures by Fracture Mechanics*, Rilem Report 6, eds. L. Elfgren & S. P. Shah, Chapman & Hall, London, 171-178.
4. van Mier, J.G.M. (1986): Multi-axial Strain-Softening of Concrete. *Materials and Structures* **19**, No. 111, Rilem, pp. 179-200.
5. Vonk, R. A. (1993). A Micromechanical Investigation of Softening of Concrete loaded in Compression. *Heron* **38**, No. 3.
6. Jansen, D.C. and S.F. Shah (1997): Effect of Length on Compressive Strain Softening of Concrete. *Journal of Engineering Mechanics* **123**, No. 1, pp. 25-35.
7. Markeset, G. (1995): A Compressive Softening Model for Concrete. In: *Fracture Mechanics of Concrete Structures*, Proceedings FRAMCOS-2, edited by Folker H. Wittmann.
8. Henriksen, M.S. and R. Brincker (1998): Modelling the Rotational Capacity of Heavily Reinforced Concrete Beams. To be published in Nordic Concrete Research, Publication No. 21.

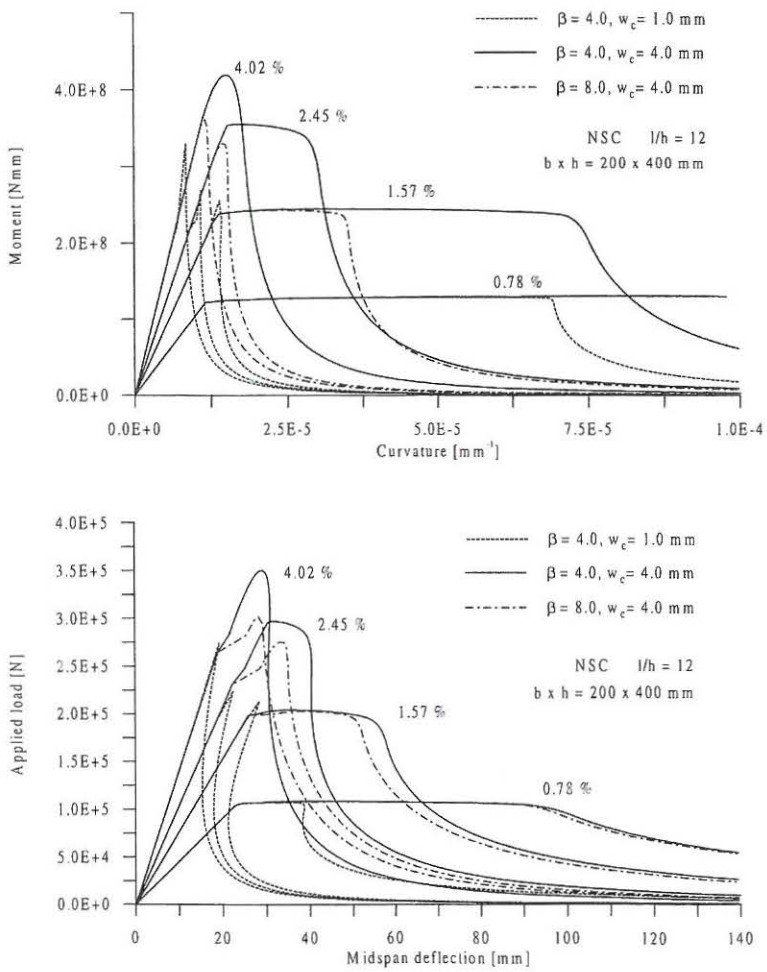

Figure D7. Model results for moment-curvature (top) and load-deflection (bottom) relation for a normal strength concrete beam (200 × 400 × 4800 mm) and different values of w_c and β.

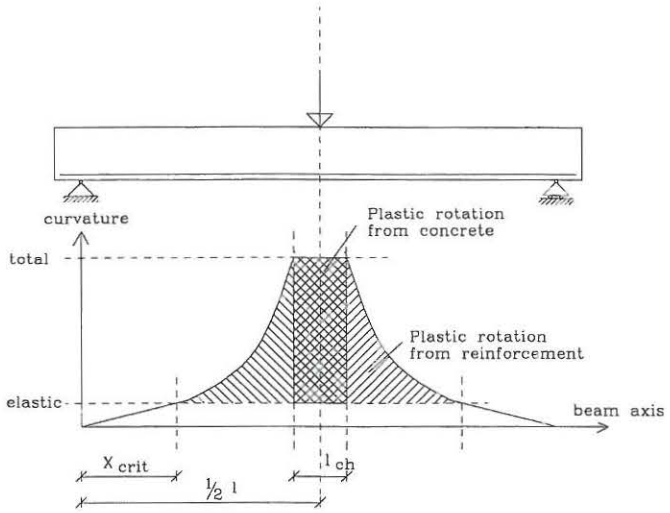

Figure D8. Typical curvature distribution along the beam axis for a beam at ultimate load.

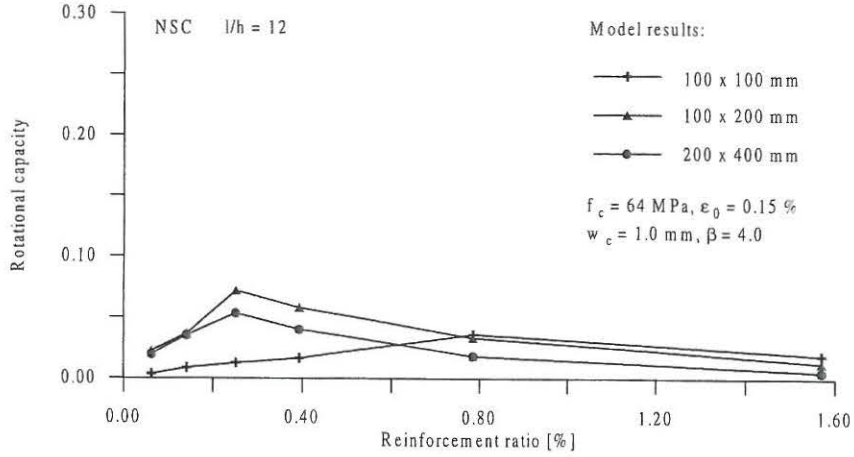

Figure D9. Model results for normal strength concrete beams with $w_c = 1.0\ mm$ and $\beta = 4.0$.

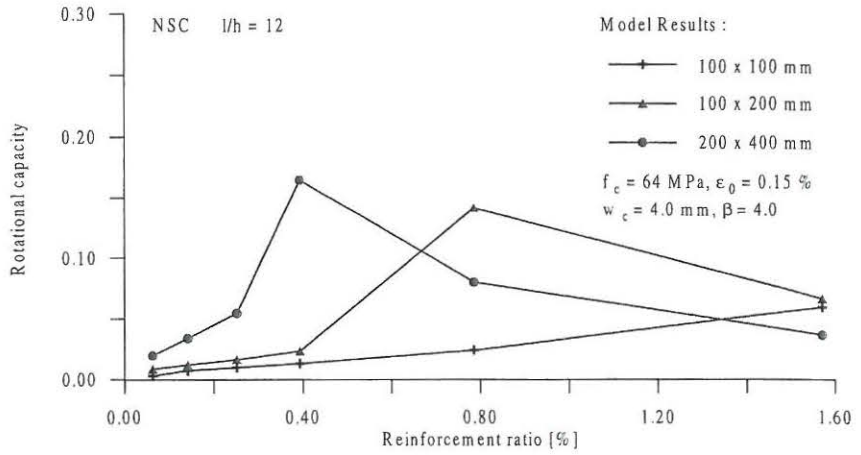

Figure D10. Model results for normal strength concrete beams with $w_c = 4.0\ mm$ and $\beta = 4.0$.

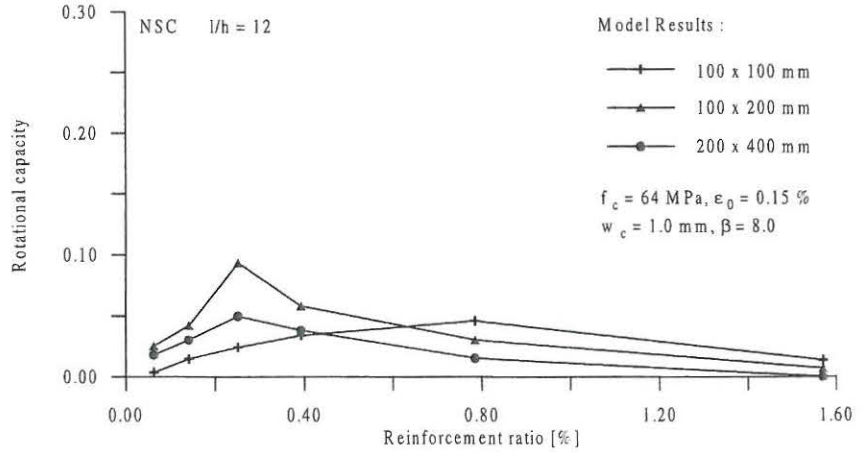

Figure D11. Model results for normal strength concrete beams with $w_c = 1.0\ mm$ and $\beta = 8.0$.

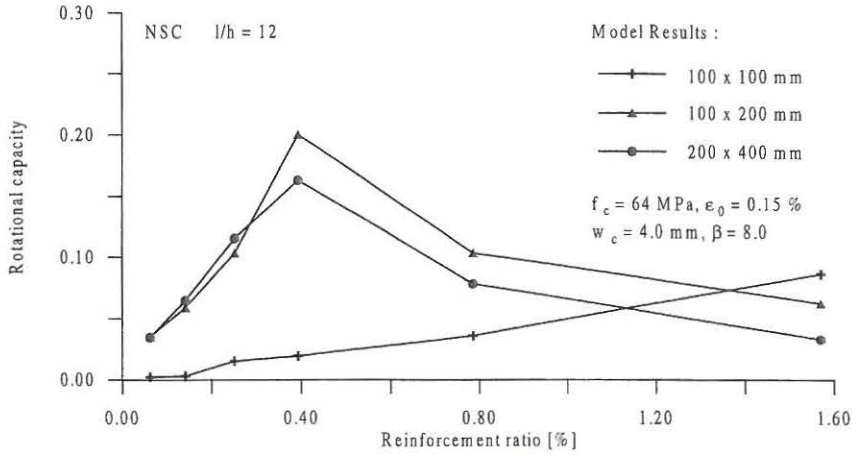

Figure D12. Model results for normal strength concrete beams with $w_c = 4.0\ mm$ and $\beta = 8.0$.

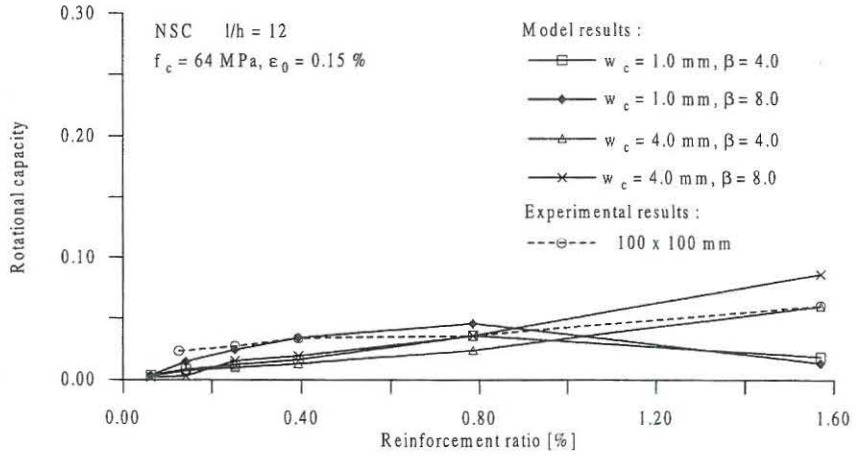

Figure D13. Results for $100 \times 100 \times 1200\ mm$ normal strength concrete beams.

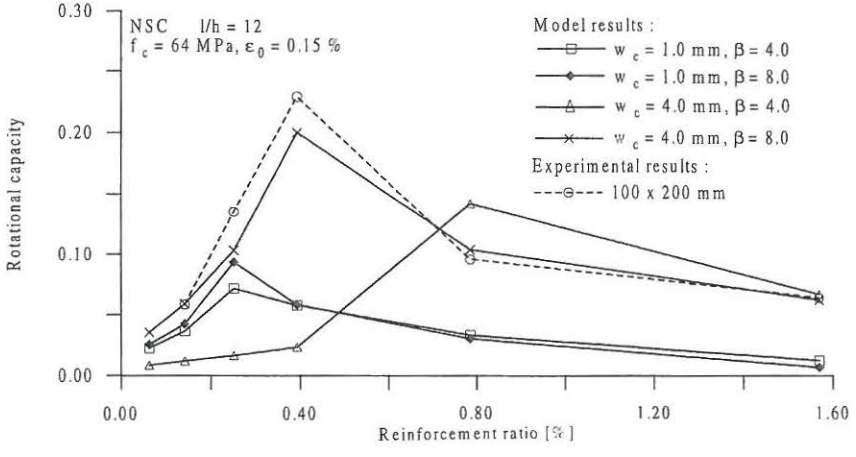

Figure D14. Results for $100 \times 200 \times 2400\ mm$ normal strength concrete beams.

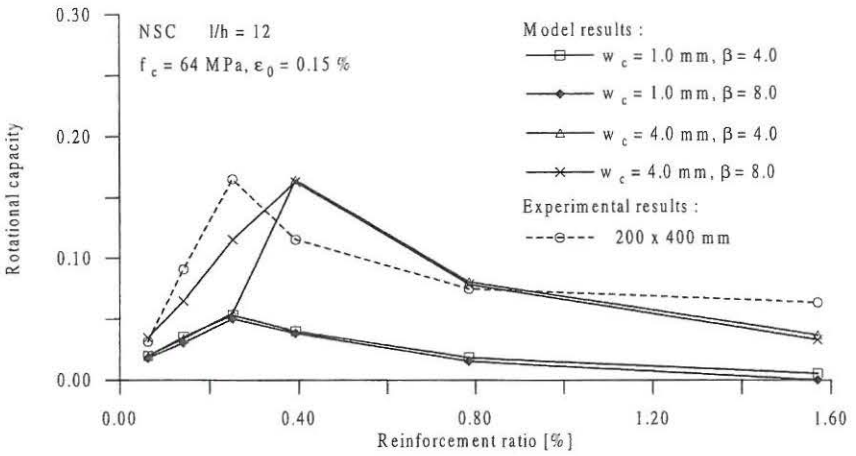

Figure D15. Results for $200 \times 400 \times 4800\ mm$ normal strength concrete beams.

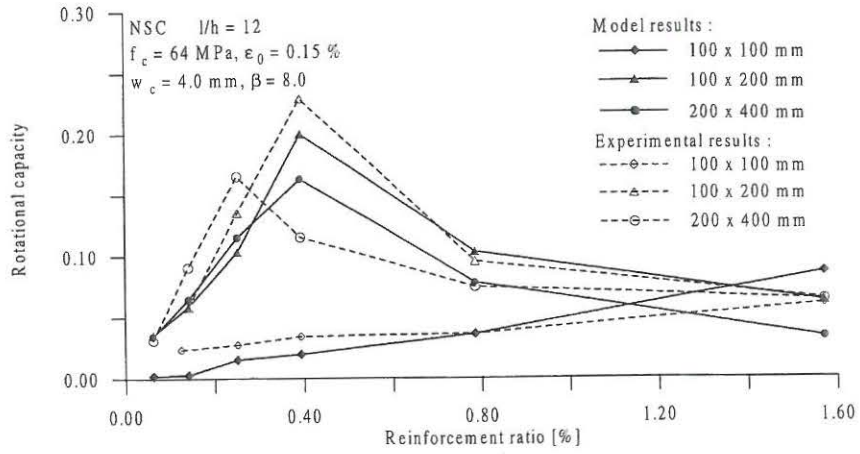

Figure D16. Results for normal strength concrete beams with $w_c = 4.0\ mm$ and $\beta = 8.0$.

MINIMUM REINFORCEMENT REQUIREMENT FOR RC BEAMS

J. OZBOLT and M. BRUCKNER
Institut für Werkstoffe im Bauwesen, Universität Stuttgart,
Pfaffenwaldring 4, D-70550 Stuttgart, Germany

ABSTRACT

In the present paper different aspects of the requirement for the minimum reinforcement ratio are studied and discussed. The influence of the beam depth is investigated in more detail. Numerical analysis for reinforced concrete beams of different sizes is carried out using plane finite element code *MASA2* which is based on the nonlocal mixed constrained microplane model. Presently, an extensive test project for reinforced concrete beams in which the material and geometrical properties are varied is in progress. Currently available test results are compared with the numerical results. It is concluded that the requirement on the minimum reinforcement depends on the beam size but also on the material properties as well as on the amount and type of the distributed reinforcement. To define the dependency between the minimum reinforcement and geometrical as well as material parameters in more detail, further theoretical and experimental studies are needed.

KEYWORDS

Minimum reinforcement, RC beams, nonlocal microplane model, energy criteria.

INTRODUCTION

In engineering practice RC beams of different sizes and with different reinforcement ratios are often used. They are normally designed such that the internal forces as well as their distribution over the cross section are calculated according to the elastic beam theory. On the contrary, the dimensioning is performed using a limit state procedure. Obviously, this is in contradiction. Therefore, significant efforts have recently been made in order to develop consistent tools and recommendations for the nonlinear structural analysis and dimensioning according to the limit state procedure. In order to provide enough structural safety and to make a redistribution of internal forces possible, RC beams must be designed such that they fail in a ductile manner. Some recent fracture mechanics studies [1-5] indicated that larger beams are more brittle than smaller. Consequently, the question is whether the same material laws and design rules may be used for RC beams of different sizes.

An important condition for ductile failure of RC beams is the minimum reinforcement requirement. The minimum reinforcement must assure a stable and ductile beam response after the concrete tensile strength at the beam tensile zone is reached. Presently, in almost all design codes the minimum reinforcement requirement is independent of the beam depth. For example, according to [6] the typical